

Detecting the effects of quantum gravity with exceptional points in optomechanical sensors

Dianzhen Cui¹, T. Li¹, Jianning Li¹, Xuexi Yi^{1,2*}

¹Center for Quantum Sciences and School of Physics,
Northeast Normal University, Changchun 130024, China

²Center for Advanced Optoelectronic Functional Materials Research,
and Key Laboratory for UV Light-Emitting Materials and Technology of Ministry of Education,
Northeast Normal University, Changchun 130024, China

(Dated: June 30, 2021)

In this manuscript, working with a binary mechanical system, we examine the effect of quantum gravity on the exceptional points of the system. On the one side, we find that the exceedingly weak effect of quantum gravity can be sensed via pushing the system towards a second-order exceptional point, where the spectra of the non-Hermitian system exhibits non-analytic and even discontinuous behavior. On the other side, the gravity perturbation will affect the sensitivity of the system to deposition mass. In order to further enhance the sensitivity of the system to quantum gravity, we extend the system to the other one which has a higher-order (third-order) exceptional point. Our work provides a feasible way to use exceptional points as a new tool to explore the effect of quantum gravity.

I. INTRODUCTION

Cavity optomechanics [1], exploring the interaction between light and mechanical systems, has made a profound impact in recent years due to its wide variety of applications including optomechanical sensors. Optomechanical sensors have achieved ultrasensitive performance in gravitational wave detection [2, 3], high-precision measurements [4], detection for mass [5], acceleration [6], displacement [7], and force [8–10]. For practical applications, the optomechanical system is unavoidably coupled with its surroundings, leading to a non-Hermitian optomechanical system. Several earlier studies have shown that non-Hermitian spectral degeneracies, also known as exceptional points (EPs) [11–15], governs the dynamics of parity-time (\mathcal{PT}) symmetric system subject to environment. In contrast to level degeneracy points in Hermitian systems, the EP is associated with level coalescence, in which the eigenenergies and the corresponding eigenvectors simultaneously coalesce [16, 17]. Besides, the intriguing phenomena of EPs in unidirectional invisibility [18], topological chirality [19] and low-threshold lasers [20, 21] have been predicted.

In recent years, sensitivity enhancement of the sensor operating at EPs has been explored both theoretically [12, 22, 23] and experimentally [14, 24–26] in a number of systems including nanoparticle detector [12, 14], mass sensor [22], and gyroscope [23–25, 27]. These studies have shown that if a second-order exceptional point (EP2) where the coalescence of two levels occurs is subjected to a perturbation of strength ϵ , the frequency splitting (the energy spacing of the two levels) is typically proportional to the square root of the perturbation strength ϵ . This is the so-called complex square-root topology.

Moreover, the splitting is significantly enhanced for sufficiently small perturbation. This suggests that the use of EP can enhance the sensitivity of a quantum sensor.

In standard quantum mechanics, on the basis of Heisenberg uncertainty principle $\Delta x \Delta p \geq \frac{\hbar}{2}$ [28], the position x and the momentum p of a particle cannot be simultaneously measured to arbitrary precision, however, the uncertainty of x can reach zero in case Δp approaches infinity. This is not the case when the quantum gravity is taken into account. It has been suggested that the uncertainty relation should be modified when gravitational effects have been taken into consideration [29]. Such generalized uncertainty principle (GUP) is found in various approaches to quantum gravity, such as the finite bandwidth approach to quantum gravity [30, 31], string theory [32–36], the theory of double special relativity [37, 38], relative locality [39] and black holes [40].

The generalized Heisenberg uncertainty principle that counts the gravity effects is $\Delta x \Delta p \geq \frac{\hbar}{2}(1 + \mu \Delta p^2)$ [35].

Here $\mu = \frac{\beta_0}{(M_p c)^2} = \frac{L_p^2}{2\hbar^2}$, β_0 is a dimensionless parameter, M_p is Planck mass, $M_p c^2$ is Planck energy and L_p is Planck length. This inequality means that $\Delta x \geq L_p \sqrt{\beta_0}$. So if $\beta_0 = 1$ [41], the minimal length is equal to the Planck length (L_p) beyond which the concepts of time and space will lose their meaning. The generalized uncertainty principle (GUP) has been extensively explored in various fields, including high energy physics, cosmology and black holes [42]. Due to experiments that can test minimal length scale directly require energies much higher than that currently available, most of the work has been devoted to find *indirect evidences* of quantum gravity in high energy particle collisions and astronomical observations [43, 44].

In this manuscript, we theoretically propose the other sensing scheme to explore the effects of quantum gravity via GUP. We will consider a binary and a ternary mechanical system separately within an optomechanical

*yixx@nenu.edu.cn

cal configuration. Controlling the gain and loss of the mechanical oscillators and driving the two cavities with blue and red detuned lasers as well as manipulating the strength of the electromagnetic field (α^{in}), we can set the system into a self-sustained regime for the mechanical oscillations. In the absence of gravity perturbation, the system is controlled to be in the EP2 state. When the gravity perturbation comes, the supermodes of the system are shifted away from the EP2. The frequency splitting induced by gravitational effects can be read out in the mechanical spectrum. This result has been further extended to a third-order exceptional point (EP3) by taking a more complicated ternary mechanical system into account. Compared with the scheme utilizing EP2, optomechanical sensor based on EP3 performs better. The physics of this EP-based sensor is that the eigenvalues of non-Hermitian Hamiltonian may exhibit non-analytic and even discontinuous behavior, which in principle enables an unlimited spectral sensitivity.

The rest of this paper is organized as follows. In Sec. II, we introduce the physical model and derive a set of equation for the dynamics of our system. In Sec. III, we study the sensitivity of the system to gravity perturbation at EP2. In Sec. IV, we extend the study on the sensitivity of the system to the gravity perturbation to EP3. In Sec. V, we discuss experimental feasibility of the proposed sensing scheme and analyze the limitation of the proposed quantum gravity sensor. Finally, the conclusions are drawn in Sec. VI. In Appendix A, we present details of derivation for the effective Hamiltonian.

II. GENERAL FRAMEWORK

We start by briefly recalling the description of harmonic oscillator with mass m when the effect of gravity is taken into consideration. Afterwards we would apply this result to our model, in which the mechanical resonator is modeled as a harmonic oscillator.

A. Deformed harmonic oscillations under quantum gravity

From the aspect of commutation relation, the gravity would modify the relation leading to the generalized uncertainty principle (GUP) given in Ref. [35],

$$[x, p] = i\hbar(1 + \mu p^2). \quad (1)$$

Define [41]

$$p = (1 + \frac{1}{3}\mu\tilde{p}^2)\tilde{p}, \quad (2)$$

where x, \tilde{p} satisfying the (non deformed) canonical commutation relations $[x, \tilde{p}] = i\hbar$. It is easy to see that Eq. (2) is written up to the first order in μ (the terms of order μ^2 and higher are neglected). For a harmonic oscillator

with frequency ω and mass m , we assume that the Hamiltonian takes $H = \frac{1}{2}m\omega^2x^2 + \frac{p^2}{2m}$ [45]. In terms of \tilde{p} , the Hamiltonian of harmonic oscillator can be rewritten as

$$H = \frac{1}{2}m\omega^2x^2 + \frac{\tilde{p}^2}{2m} + \frac{\mu\tilde{p}^4}{3m}. \quad (3)$$

Introducing canonical creation and annihilation operators,

$$b^\dagger = \sqrt{\frac{m\omega}{2\hbar}}(x - \frac{i\tilde{p}}{m\omega}), b = \sqrt{\frac{m\omega}{2\hbar}}(x + \frac{i\tilde{p}}{m\omega}) \quad (4)$$

and rewriting the Hamiltonian (3) in terms of b , we can get

$$H = \hbar\omega(b^\dagger b + \frac{1}{2}) + \frac{1}{12}\hbar^2\omega^2m\mu(b - b^\dagger)^4. \quad (5)$$

The first term represents the free Hamiltonian of the harmonic oscillator. The second term comes from the gravitational effects.

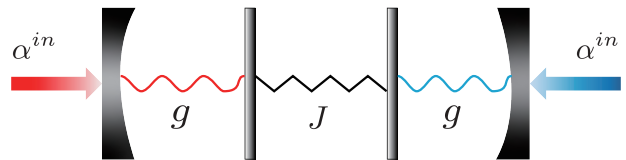


FIG. 1: Sketch of the studied system. An open system consisted of two coupled mechanical resonators. Each resonator is coupled to an optical cavity. The two cavities are driven by red- and blue-detuned pump laser, respectively.

B. Modeling and dynamical equations

We consider two coupled identical resonators with optomechanically induced gain and loss. Each of the resonators is characterized by frequency ω_j , damping rate γ_m and coupling strength J . The schematic diagram is presented in Fig. 1. In this configuration, the theory states that only the mechanical commutation relation are modified, while the optical commutation relation remains unchanged, i.e., $[a, a^\dagger] = 1$ [46]. The total Hamiltonian of the whole system can be written as ($\hbar = 1$)

$$H = H_f + H_i + H_d + H_g, \quad (6)$$

where,

$$\begin{aligned} H_f &= \sum_{j=1,2} \omega_{a,j} a_j^\dagger a_j + \omega_j b_j^\dagger b_j, \\ H_i &= \sum_{j=1,2} \{ -g a_j^\dagger a_j (b_j^\dagger + b_j) \} - J(b_1 b_2^\dagger + b_1^\dagger b_2), \\ H_d &= \sum_{j=1,2} iE(a_j^\dagger e^{-i\omega_{p,j}t} - a_j e^{i\omega_{p,j}t}), \\ H_g &= \sum_{j=1,2} \frac{1}{12} \omega_j^2 m_j \mu_j (b_j - b_j^\dagger)^4. \end{aligned} \quad (7)$$

In this expression, H_f represents the sum of free Hamiltonian of the optomechanical system, a_j^\dagger (b_j^\dagger) and a_j (b_j) are the creation and annihilation operators of the j th cavity (mechanical resonator) ($j = 1, 2$). The frequencies of the cavities and mechanical resonators are $\omega_{a,j}$ and ω_j , respectively. H_i describes the interaction Hamiltonian of the configuration. The first term represents the coupling of the cavities to the corresponding mechanical resonators with optomechanical coupling strength g . The second term describes the coupling between the two mechanical resonators with coupling strength J . H_d indicates that the two cavities are driven by external fields with amplitude E and frequency $\omega_{p,j}$. H_g describes the gravitational effects in mechanical resonators. The effective mass of the j th mechanical mode is m_j . In the frame rotating at the input laser frequency ω_p , the Hamiltonian of the system reads,

$$H = \sum_{j=1,2} \left\{ -\Delta_j a_j^\dagger a_j + \omega_j b_j^\dagger b_j - g a_j^\dagger a_j (b_j^\dagger + b_j) + \frac{1}{12} \omega_j^2 m_j \mu_j (b_j - b_j^\dagger)^4 + iE(a_j^\dagger - a_j) \right\} - J(b_1 b_2^\dagger + b_1^\dagger b_2), \quad (8)$$

where, $\Delta_j = \omega_{p,j} - \omega_{a,j}$ represents the detuning of the driving field with respect to the cavity. As we are interested in the classical limit, where photon and phonon numbers are assumed large in the model. Thus, we replace the quantum operators with their mean values, i.e., $\alpha_j = \langle a \rangle$ and $\beta_j = \langle b \rangle$. By introducing dissipation terms, the evolution of the system operators is obtained as follows [1],

$$\begin{aligned} \frac{d\alpha_j}{dt} &= [i(\Delta_j + g(\beta_j^* + \beta_j)) - \frac{\kappa}{2}] \alpha_j + \sqrt{\kappa} \alpha_j^{in}, \\ \frac{d\beta_j}{dt} &= -(i\omega_j + \frac{\gamma_m}{2}) \beta_j + iJ\beta_{3-j} + ig\alpha_j^* \alpha_j \\ &\quad + \frac{1}{3} im_j \omega_j^2 \mu_j (\beta_j - \beta_j^*)^3, \end{aligned} \quad (9)$$

where κ and γ_m are the intrinsic damping rates of the cavities and mechanical resonators, respectively. $E =$

$\sqrt{\kappa} \alpha_j^{in}$ is the amplitude of the driving field, where $\alpha_j^{in} = \sqrt{\frac{p_{in}}{\hbar \omega_{p,j}}}$ characterizes the input field driving the cavity. For the sake of simplicity, we assume the two cavities and mechanical resonators identical, this means $\omega_j = \omega_m$, $m_j = m$, and $\mu_j = \mu$. We apply the input lasers with the same power (p_{in}) to drive the two mechanical resonators, i.e., $\alpha_j^{in} = \alpha^{in}$. Throughout the work, the parameters satisfy the following condition, $\gamma_m, g \ll \kappa \ll \omega_m$, similar to those chosen in Ref. [47, 48]. Under this hierarchy, the amplitude and phase of the mechanical resonators slowly evolving on the time scale of the cavity dynamics.

We will pay our attention to the steady state of the mechanical resonators. In this regime, $\beta_j(t) = \beta_j + B_j e^{-i\theta} e^{-i\omega_l t}$ [49, 50], where β_j is the center of the mechanical oscillations and amplitude B_j can be regarded as a slowly evolving function of time. In the limit-cycle states, both mechanical resonators start oscillating with a locked frequency (ω_l). On this point, it can be seen from its Fourier spectrum, where the peak of the spectrum is much larger than the corresponding amplitude of other frequency components [51]. Throughout this paper, we set $\theta = 0$. In parallel, we removed all terms in mechanical dynamics except for the constant one and the term oscillating at ω_l . Using this analytic approximation, we solve the equation for α_j assuming a fixed mechanical amplitude and then substitute the result into the equation for β_j , resulting in the following set of equations of motion describing this effective mechanical system (see Appendix A):

$$\begin{aligned} \frac{d\beta_1}{dt} &= -(i\omega_{eff}^1 + \frac{\gamma_{eff}^1}{2} + i\Theta_1) \beta_1 + iJ\beta_2 + i\Theta_1 \beta_1^*, \\ \frac{d\beta_2}{dt} &= -(i\omega_{eff}^2 + \frac{\gamma_{eff}^2}{2} + i\Theta_2) \beta_2 + iJ\beta_1 + i\Theta_2 \beta_2^*, \end{aligned} \quad (10)$$

where, $\Theta_j = \mu m \omega_j^2 B_j^2$ ($j = 1, 2$). $\omega_{eff}^j = \omega_j + \Omega_j$ and $\gamma_{eff}^j = \gamma_m + \Gamma_j$ ($j = 1, 2$) represent the effective frequency and damping of the j th mechanical oscillator ($j = 1, 2$), respectively. The modal field evolution in this configuration obeys $i \frac{d\phi}{dt} = H_{eff} \phi$, where $\phi = (\beta_1, \beta_2, \beta_1^*, \beta_2^*)^T$ is the state vector and t represents time. H_{eff} is the associated 4×4 non-Hermitian Hamiltonian (see more details in Appendix A):

$$H_{eff} = \begin{pmatrix} \omega_{eff}^1 - i\frac{\gamma_{eff}^1}{2} + \Theta_1 & -J & -\Theta_1 & 0 \\ -J & \omega_{eff}^2 - i\frac{\gamma_{eff}^2}{2} + \Theta_2 & 0 & -\Theta_2 \\ \Theta_1 & 0 & -\omega_{eff}^1 - i\frac{\gamma_{eff}^1}{2} - \Theta_1 & J \\ 0 & \Theta_2 & J & -\omega_{eff}^2 - i\frac{\gamma_{eff}^2}{2} - \Theta_2 \end{pmatrix}. \quad (11)$$

Here, Ω_j (Γ_j) represents the optical spring effect (the optomechanical damping rate). These quantities are given

as (see more details in Appendix A)

$$\Omega_j = -\frac{2\kappa(g\alpha^{in})^2}{\omega_l \epsilon_j} \text{Re} \left(\sum_n \frac{J_{n+1}(-\epsilon_j) J_n(-\epsilon_j)}{K_{n+1}^{j*} K_n^j} \right), \quad (12)$$

and

$$\Gamma_j = \frac{2(g\kappa\alpha^{in})^2}{\epsilon_j} \sum_n \frac{J_{n+1}(-\epsilon_j)J_n(-\epsilon_j)}{|K_{n+1}^{j*}K_n^j|^2}. \quad (13)$$

Firstly, we focus on the case without gravitational effect, the eigenvalues of the above effective Hamiltonian are given by

$$\lambda_{\pm} = \omega_l - \frac{i}{4}(\gamma_{eff}^1 + \gamma_{eff}^2) \pm \frac{1}{4}\delta, \quad (14)$$

where,

$$\delta = \sqrt{16J^2 + [2(\omega_{eff}^1 - \omega_{eff}^2) + i(\gamma_{eff}^2 - \gamma_{eff}^1)]^2}. \quad (15)$$

Here, $\omega_l = \frac{\omega_{eff}^1 + \omega_{eff}^2}{2}$. Replace the conventional vibrational modes, we now have new mechanical modes, which can be called as the mechanical supermodes. The effective frequencies and spectral linewidths of the system are defined as the real (ω) and imaginary (γ) parts of eigenvalues, respectively. The solid lines in Fig. 2 show the real and imaginary parts of the eigenvalues *vs* the driving strength α^{in} before the perturbation introduced by gravity effects. At the specific point, both these pairs of effective frequencies and effective dampings of the system coalesce. It is evident that for a critical driving strength

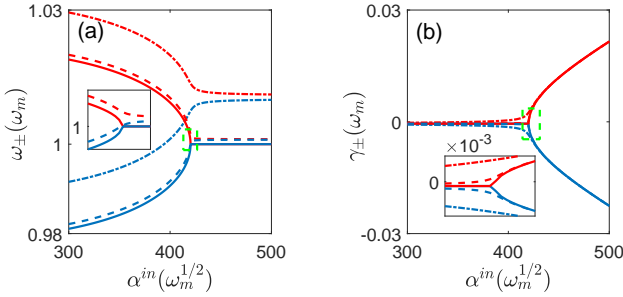


FIG. 2: (a) The real and (b) the imaginary parts of the eigenvalues *vs* the driving strength α^{in} before and after the perturbation introduced by gravitational effects. The system exhibits an EP2 at $4J = \gamma_{eff}^2 - \gamma_{eff}^1$. The green dashed box is zoomed out in the inset to show the influence of gravitational effects on EP2. Each panel contains various curves for comparison: the solid lines denote the eigenvalues without gravitational effect, the dashed lines indicate the eigenvalues at $\mu m = (0.02 \times 2.2 \times 10^{-7})\omega_m^{-1}$, and the dash-dotted lines represent the eigenvalues at $\mu m = (0.02 \times 2.2 \times 10^{-6})\omega_m^{-1}$. The other parameters are chosen as $J = 2.2 \times 10^{-2}\omega_m$, $g = 2.5 \times 10^{-4}\omega_m$, $\gamma_m = 10^{-3}\omega_m$, $\kappa = 10^{-1}\omega_m$, $\omega_1 = \omega_2 = \omega_m$, $\Delta_1 = -\omega_m$, and $\Delta_2 = \omega_m$. The colors (red, blue) represent a pair of eigenvalues of our model.

α^{in} the pairs of eigenvalues merge at $4J = \gamma_{eff}^2 - \gamma_{eff}^1$.

III. SENSITIVITY AT THE SECOND-ORDER EXCEPTIONAL POINT

A. Sensitivity of a system at the second-order exceptional point to the gravity effect

For the case with gravitational effects, we numerically solve the eigenvalues of this mechanical effective Hamiltonian and show the results in Fig. 2. The effective Hamiltonian has 4 eigenvalues forming two pairs, one pair is due to the appearance of β_j^* in the dynamics.

As shown in Fig. 2, we see that the splitting of effective frequency (real part of the eigenvalue) and linewidth (imaginary part of the eigenvalue) increases as the mass of the mechanical resonators increases. This is attributed to the fact that gravity effect is enhanced by larger system mass. A typical detection strategy is to observe the associated mode response, usually the frequency splitting or the frequency shift, before and after the perturbation induced by gravitational effects taking place. In this paper, in order to quantify the frequency splitting caused by the gravity effect, we define the sensitivity as follows,

$$\Delta\omega = |Re\lambda_+ - Re\lambda_-|. \quad (16)$$

The perturbation of gravitational effects can shift the EP2, and thereby the degeneracy of the effective frequencies are released and cause the supermodes to split. The

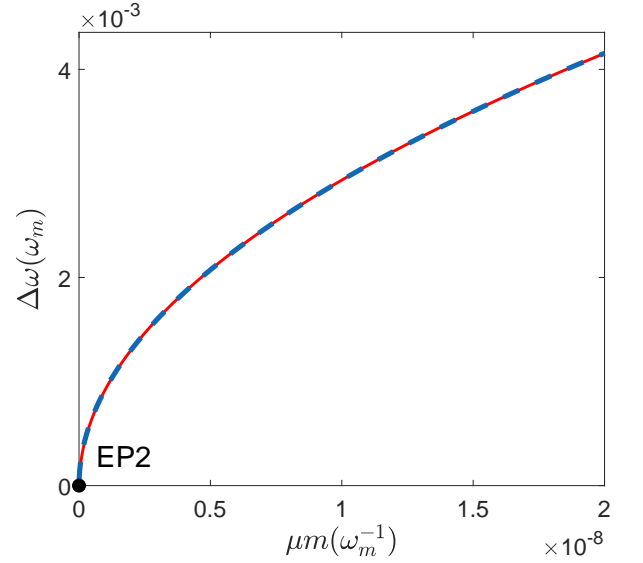


FIG. 3: Sensitivity (red solid line) at the second-order EP *vs* μm . The blue dashed line denotes the fitted curve with $\xi = 30.12\omega_m^{3/2}$. The parameters are the same as that in Fig. 2.

frequency splitting caused by gravitational effects can be fitted using

$$\Delta\omega \approx \xi(\mu m)^{1/2}. \quad (17)$$

Here, ξ is the fitting coefficient. Fig. 3 shows $\Delta\omega$ as a function of the μm near the EP2. The blue dashed lines

represent the fitting result according to Eq. (17) with $\xi = 30.12\omega_m^{3/2}$, which is consistent with the mechanical frequency splitting in our model. Therefore, it can be inferred that the mechanical frequency splitting in response to the μm obeys the square root behavior. Due to the intrinsic properties of EP2, we can claim that the sensitivity is significantly enhanced by exploiting EP2 for sufficiently small perturbation strength, proving the efficiency of the EP2 sensor in detecting gravity effect.

B. Sensitivity of the system to deposition mass at the second-order exceptional point with gravity effect

In order to gain insight into the influence of gravity effects on mass sensing, we assume that a mass δm has been deposited on the mechanical oscillator driven by the blue-detuned electromagnetic field, which would induce the frequency shift given in Eq. (14), i.e., replacing ω_{eff}^2 with $\omega_{eff}^2 + \delta\omega$. For an ordinary mass sensor, the relation between the deposited mass δm and the frequency shift $\delta\omega$ is given by [52]

$$\delta m = \frac{2m}{\omega_m} \delta\omega = \zeta^{-1} \delta\omega, \quad (18)$$

where ζ represents the mass responsivity of the mechanical resonator. We can define the gap as

$$\chi_{\pm} = \lambda_{\pm}(m) - \lambda_{\pm}. \quad (19)$$

Figure 4 shows that for mechanical frequency shift

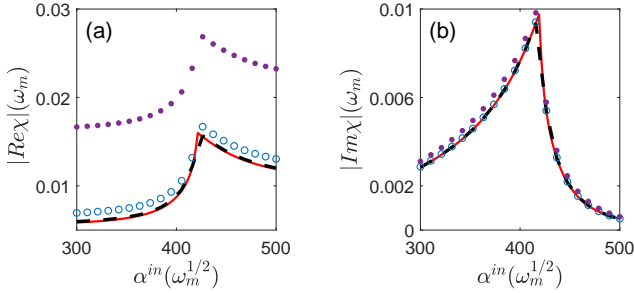


FIG. 4: (a) The real and (b) the imaginary parts of χ vs α^{in} before and after the perturbation induced by gravitational effects with frequency shift $\delta\omega = 10^{-2}\omega_m$. Each panel contains various lines for comparison. The red solid lines denote the gap without gravitational effect, the black dashed lines indicate the gap at $\mu m = (0.02 \times 2.2 \times 10^{-8})\omega_m^{-1}$, the blue circles represent the eigenvalues at $\mu m = (0.02 \times 2.2 \times 10^{-7})\omega_m^{-1}$, and the purple filled circles mean the eigenvalues at $\mu m = (0.02 \times 2.2 \times 10^{-6})\omega_m^{-1}$. Other system parameters are the same as that in Fig. 2. Note these results are for χ_+ .

$\delta\omega = 10^{-2}\omega_m$, the larger the mass of the mechanical resonators, the larger the gap between effective frequencies before and after gravitational effects being considered. However, the gap between the effective dampings

(the imaginary part of the eigenvalues) does not change significantly. Therefore, small mass of the mechanical resonators can decrease the disturbance caused by gravitational effects.

IV. SENSITIVITY OF A SYSTEM AT THE THIRD-ORDER EXCEPTIONAL POINT TO THE GRAVITY EFFECT

Inspired by these results, we now extend this scheme to the higher-order exceptional points (EPs). A possible configuration that supports a third-order exceptional point (EP3) would be a system consisting of two cavities and three coupled mechanical oscillators where the two cavities are symmetrically driven by red- and blue-detuned lasers, and the corresponding mechanical resonators are coupled together (see Fig. 5). Proceeding in

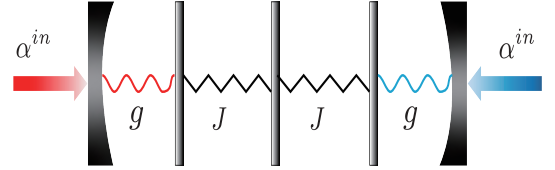


FIG. 5: A schematic diagram of model. An system consisted of coupled ternary resonators.

a similar way, one can write the following the Hamiltonian of the system,

$$H = H_f + H_i + H_d + H_g, \quad (20)$$

with

$$\begin{aligned} H_f &= \sum_{j=1,2} -\Delta_j a_j^\dagger a_j + \sum_{j=1,2,3} \omega_j b_j^\dagger b_j, \\ H_i &= -g a_1^\dagger a_1 (b_1^\dagger + b_1) - g a_2^\dagger a_2 (b_3^\dagger + b_3) \\ &\quad - J(b_1 b_2^\dagger + b_1^\dagger b_2) - J(b_2 b_3^\dagger + b_2^\dagger b_3), \\ H_d &= \sum_{j=1,2} iE(a_j^\dagger - a_j), \\ H_g &= \sum_{j=1,2,3} \frac{1}{12} \omega_j^2 m_j \mu_j (b_j - b_j^\dagger)^4. \end{aligned} \quad (21)$$

From Eq. (21), one can write the following nonlinear equations of motion,

$$\begin{aligned} \frac{d\alpha_j}{dt} &= [i(\Delta_j + g(\beta_j^* + \beta_j)) - \frac{\kappa}{2}] \alpha_j + \sqrt{\kappa} \alpha_j^{in}, \\ \frac{d\beta_1}{dt} &= -(i\omega_1 + \frac{\gamma_m}{2}) \beta_1 + iJ\beta_2 + ig\alpha_1^* \alpha_1 + \Xi_1 (\beta_1 - \beta_1^*)^3, \\ \frac{d\beta_2}{dt} &= -(i\omega_2 + \frac{\gamma_m}{2}) \beta_2 + iJ\beta_1 + iJ\beta_3 + \Xi_2 (\beta_2 - \beta_2^*)^3, \\ \frac{d\beta_3}{dt} &= -(i\omega_3 + \frac{\gamma_m}{2}) \beta_3 + iJ\beta_2 + ig\alpha_2^* \alpha_2 + \Xi_3 (\beta_3 - \beta_3^*)^3. \end{aligned} \quad (22)$$

Here, $\Xi_j = \frac{1}{3}i\mu m\omega_j^2$ ($j = 1, 2, 3$), $\alpha_j = \langle a_j \rangle$ ($j = 1, 2$), and $\beta_j = \langle b_j \rangle$ ($j = 1, 2, 3$). For the convenience of discussion, we assume $\omega_j = \omega_m$ ($j = 1, 2, 3$).

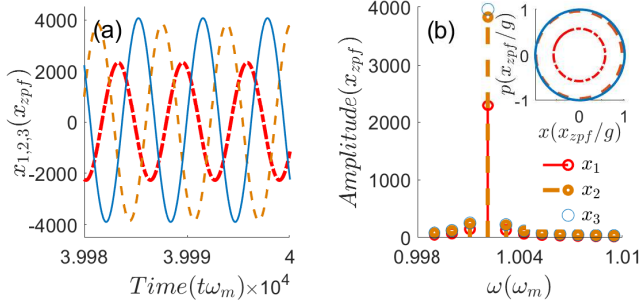


FIG. 6: (a) The time evolution of the three resonators with $\alpha^{in} = 160\sqrt{\omega_m}$. Red dash-dotted, orange dashed, and blue solid lines for different resonators. (b) Fourier spectra and its corresponding phase space trajectories. The coupling has been fixed at $J = 2.2 \times 10^{-3}\omega_m$, and the other parameters are the same as in Fig. 2.

In Fig. 6, we show the overall properties of the steady

state solutions of the mechanical resonators. It is easy to find that the amplitudes of the the mechanical resonators change very slowly over time [see Fig. 6 (a)]. Fig. 6 (b) shows the corresponding Fourier spectra. It is easy to see that all three mechanical resonators start oscillating with a same frequency, i.e., $\omega_l = \frac{\omega_{eff}^1 + \omega_2 + \omega_{eff}^3}{3}$. The inset of Fig. 6 (b) shows limit cycle oscillations at $\alpha^{in} = 160\sqrt{\omega_m}$ and $J = 2.2 \times 10^{-3}\omega_m$. So in this case, the formal solution for $\beta_j(t)$ is still applicable. By the use of this formal solution, Eq. (22) can be further reduced to

$$\begin{aligned} \frac{d\beta_1}{dt} &= -(i\omega_{eff}^1 + \frac{\gamma_{eff}^1}{2} + i\Theta_1)\beta_1 + iJ\beta_2 + i\Theta_1\beta_1^*, \\ \frac{d\beta_2}{dt} &= -(i\omega_2 + \frac{\gamma_m}{2} + i\Theta_2)\beta_2 + iJ\beta_1 + iJ\beta_3 + i\Theta_2\beta_2^*, \\ \frac{d\beta_3}{dt} &= -(i\omega_{eff}^3 + \frac{\gamma_{eff}^3}{2} + i\Theta_3)\beta_3 + iJ\beta_2 + i\Theta_3\beta_3^*. \end{aligned} \quad (23)$$

Here $\Theta_j = \mu m\omega_j^2 B_j^2$ ($j = 1, 2, 3$). The modal field evolution in this configuration obeys $i\frac{d\psi}{dt} = H_{eff}\psi$, where $\psi = (\beta_1, \beta_2, \beta_3, \beta_1^*, \beta_2^*, \beta_3^*)^T$ represents the modal state vector and t represents time. H_{eff} is the associated 6×6 non-Hermitian Hamiltonian,

$$\begin{pmatrix} \omega_{eff}^1 - i\frac{\gamma_{eff}^1}{2} + \Theta_1 & -J & 0 & -\Theta_1 & 0 & 0 \\ -J & \omega_2 - i\frac{\gamma_m}{2} + \Theta_2 & -J & 0 & -\Theta_2 & 0 \\ 0 & -J & \omega_{eff}^3 - i\frac{\gamma_{eff}^3}{2} + \Theta_3 & 0 & 0 & -\Theta_3 \\ \Theta_1 & 0 & 0 & -\omega_{eff}^1 - i\frac{\gamma_{eff}^1}{2} - \Theta_1 & J & 0 \\ 0 & \Theta_2 & 0 & J & -\omega_2 - i\frac{\gamma_m}{2} - \Theta_2 & J \\ 0 & 0 & \Theta_3 & 0 & J & -\omega_{eff}^3 - i\frac{\gamma_{eff}^3}{2} - \Theta_3 \end{pmatrix}. \quad (24)$$

It is easy to find that the effective Hamiltonian has 6 eigenvalues forming two pairs, one pair is due to the appearance of β_j^* in the dynamics. This characteristic feature of the EP3 has been demonstrated in Fig. 7 (a) and (b), where we show the dependence of the eigenvalues on driving strength α^{in} .

Now to take this discussion further to show how the system reacts around the EP3. The real [Fig. 7 (c)] and imaginary parts [Fig. 7 (d)] of the eigenvalues are plotted as a function of μm . Moreover, it is easy to see that the power (p_{in}) required to reach the third-order exceptional point is lower than that required by EP2.

The difference between two effective frequencies (in this case, ω_2 and ω_3) is also plotted (Fig. 8) as a function of μm . The frequency splitting caused by μm can be fitted using

$$\Delta\omega \approx \zeta(\mu m)^{1/3}. \quad (25)$$

Here ζ is the fitting coefficient. The blue dashed line represents the fitting results according to Eq. (25) with

$\zeta = 2.874\omega_m^{4/3}$, which is consistent with the mechanical frequency splitting in our system, confirming thus that the mechanical frequency splitting in response to μm obeys the cube root behavior. This indicates that it is feasible to further enhance the sensitivity by means of third-order exceptional point (EP3).

V. EXPERIMENTAL FEASIBILITY AND ULTIMATE LIMITS OF THE SENSING SCHEME

There are many types of optomechanical systems. For concreteness, we choose one of them, where the mechanical degree of freedom is a dielectric membrane placed inside a Fabry-Perot cavity [53]. Here we use two coupled Si beams, which possess the mass of $m = 5.3 \times 10^{-3}$ ng and thickness $t = 80$ nm [54]. Here we take the EP2-based sensor as an example, as shown in Fig. 9 (a) and (b). In general, various basic physical noise processes will limit the sensitivity of the sensing scheme. For the

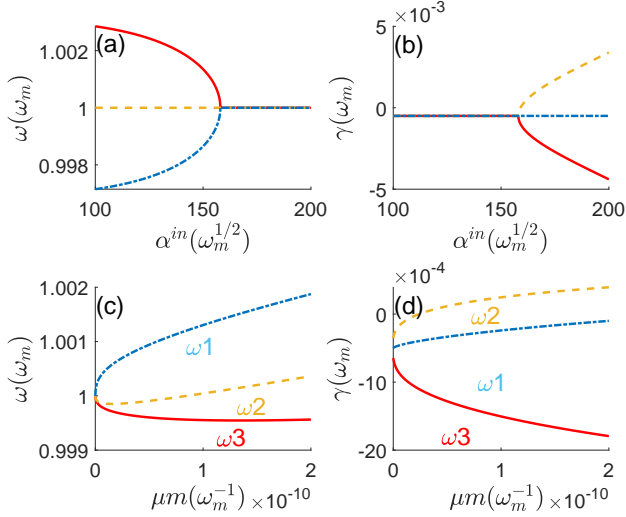


FIG. 7: (a) The real and (b) the imaginary parts of the eigenvalues as a function of the driving strength α^{in} before the perturbation introduced by gravitational effects, where the corresponding mechanical coupling strength $J = 2.2 \times 10^{-3} \omega_m$. (c) The real and (d) the imaginary parts of the eigenvalues of the ternary mechanical system as a function of μm around a third-order exceptional point for a fixed $J = 2.2 \times 10^{-3} \omega_m$. The three eigenvalues of the effective Hamiltonian are marked with red solid, orange dashed, and blue dash-dotted lines. The other system parameters are the same as in Fig. 2.

nanomechanical resonators, the main noise source is the thermomechanical noise [54]. In order to obtain this basic limits imposed upon measurements by thermomechanical fluctuations, we need to consider the minimum detectable frequency shift ($\delta\omega$) that can be resolved in a practical noisy system. An estimate for $\delta\omega$ can be obtained by [54]

$$\delta\omega \approx \left(\frac{K_B T}{E_c} \frac{\omega_n \Delta f}{Q} \right)^{1/2}. \quad (26)$$

Here Q is the mechanical quality factor, K_B is the Boltzmann constant, T is the effective temperature of the mechanical resonator, and $E_c = m\omega_m^2 \langle x_c^2 \rangle$, which describes the maximum drive energy. $\langle x_c^2 \rangle$ can be approximated as [54]

$$\langle x_c^2 \rangle \approx 0.53t. \quad (27)$$

In order to obtain the ultimate sensitivity limits of the system to the effect of gravity, we assume that the frequency splitting caused by gravitational effects is exactly equal to the minimum measurable frequency shift ($\delta\omega$) determined by the thermomechanical fluctuations, i.e., $\Delta\omega_{min} = \delta\omega$. We plot $\Delta\omega_{min}$ as a function of the bandwidth for thermomechanical fluctuations in Fig. 9 (c). The result shows that small bandwidth Δf and high quality factor Q of the mechanical resonator are essential for the superresolution. Assuming that $\Delta f = 10^{-10}$ Hz, we can obtain the quantum-noise-limited sensitiv-

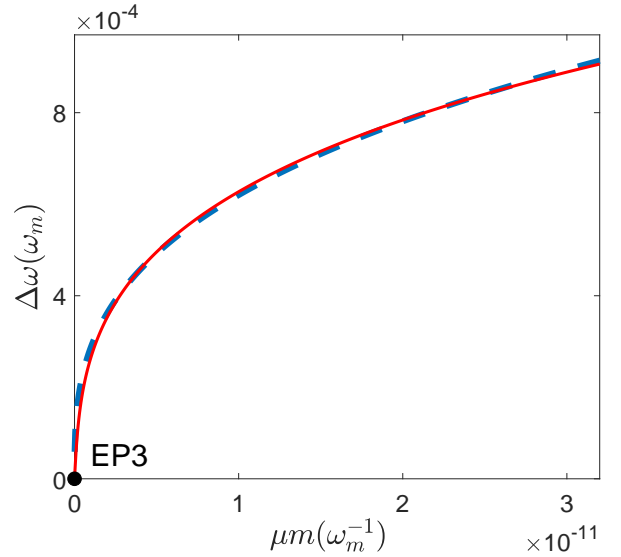


FIG. 8: Frequency splitting (red solid line) in the mechanical supermodes *vs* μm near EP3 for $J = 2.2 \times 10^{-3} \omega_m$. The blue dashed line denotes the fitted curve with $\zeta = 2.874 \omega_m^{4/3}$. The other parameters are the same as in Fig. 2.

ity of the system to gravitational effects with Eq.(26), $\Delta\omega_{min} \sim 10^{-12}$ Hz for $Q = 10^{12}$.

VI. CONCLUSION

In conclusion, we have presented a scheme for sensing the effect of quantum gravity. Starting with a system consisting of two coupled resonators with driving and dissipation, we show that the system eigenenergy is sensitive to the effect of quantum gravity when the system is in an second-order exceptional point. The response of the binary mechanical system to the gravity exhibits square root behaviour, and the sensitivity of the system at EPs increases significantly with the decrease of the perturbation. Moreover, we found that small mass of the mechanical resonator benefits the sensitivity of the system to deposition mass. In order to further enhance the sensitivity of the system to the effect of gravity, we extend the sensing scheme to a third-order exceptional point by taking a more complicated ternary mechanical system into account. The response of the ternary mechanical systems to perturbation exhibits cube root behaviour. The quantum-noise-limited sensitivity of the system to gravitational effects due to thermomechanical noise is also discussed. It is worthwhile to note that our scheme could, in principle, be extended to various photonic and phononic systems with optomechanically induced gain and loss. These findings may pave the ways for utilizing EPs as a novel tool to probe effect of quantum gravity.

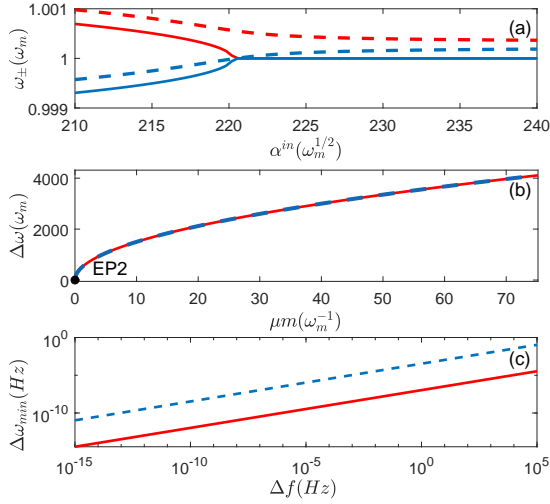


FIG. 9: (a) The real parts of the eigenvalues *vs* the driving strength α^{in} before perturbation (solid lines) and after perturbation (dashed lines) by gravitational effects with $\mu m = (0.02 \times 10^{-19})\omega_m^{-1}$. The two eigenvalues of our model are marked with red and blue lines. (b) Frequency splitting in the mechanical supermodes *vs* μm near EP2. The blue dashed line denotes the fitted line, where the fitting coefficient is $\xi = 474.1\omega_m^{3/2}$. (c) Limit of the sensitivity of the system to gravitational effects imposed by thermomechanical noise as a function of the bandwidth with $Q = 10^{12}$ (red solid line) and $Q = 10^5$ (blue dashed line) in the condition of $T = 300K$. The experimentally realistic parameters are chosen as $\omega_m/2\pi = 6$ GHz, $\gamma_m/2\pi = 3$ MHz, $g/2\pi = 0.8$ MHz, $\kappa/2\pi = 2$ GHz, and $J/2\pi = 10$ MHz [55].

VII. ACKNOWLEDGMENTS

This work is supported by National Natural Science Foundation of China (NSFC) under Grants No. 11775048 and No. 11947405.

Appendix A: the derivation of mechanical effective Hamiltonian

Based on this formal solution: $\beta_j(t) = \bar{\beta}_j + B_j e^{-i\theta} e^{-i\omega_l t}$ ($\bar{\beta}_j \ll B_j$) [49, 50], Eq. (9) can be further simplified as

$$\begin{aligned} \frac{d\beta_1}{dt} &= -(i\omega_1 + \frac{\gamma_m}{2})\beta_1 + iJ\beta_2 + ig\alpha_1^* \alpha_1 + i\Theta_1(-\beta_1 + \beta_1^*), \\ \frac{d\beta_2}{dt} &= -(i\omega_2 + \frac{\gamma_m}{2})\beta_2 + iJ\beta_1 + ig\alpha_2^* \alpha_2 + i\Theta_2(-\beta_2 + \beta_2^*), \end{aligned} \quad (A1)$$

$$H_{eff} = \begin{pmatrix} \omega_{eff}^1 - i\frac{\gamma_{eff}^1}{2} + \Theta_1 & -J & -\Theta_1 & 0 \\ -J & \omega_{eff}^2 - i\frac{\gamma_{eff}^2}{2} + \Theta_2 & 0 & -\Theta_2 \\ \Theta_1 & 0 & -\omega_{eff}^1 - i\frac{\gamma_{eff}^1}{2} - \Theta_1 & J \\ 0 & \Theta_2 & J & -\omega_{eff}^2 - i\frac{\gamma_{eff}^2}{2} - \Theta_2 \end{pmatrix}. \quad (A7)$$

where, $\Theta_j = \mu m \omega_j^2 B_j^2$ ($j = 1, 2$). We substitute this formal solution into the equation for α_j , one then obtain the dynamics of the cavity field in the form,

$$\alpha_j(t) = \exp(-i\varphi_j(t)) \sum_n A_n^j \exp(in\omega_l t), \quad (A2)$$

with

$$A_n^j = \sqrt{\kappa} \alpha^{in} \frac{J_n(-\epsilon_j)}{K_n^j}, \quad (A3)$$

where $\epsilon_j = 2gB_j/\omega_l$ is normalized amplitude, $\Delta_j' = \Delta_j + 2gRe(\bar{\beta}_j)$, $K_n^j = i(n\omega_l - \Delta_j') + \frac{\kappa}{2}$, the global phase is $\varphi(t) = -\epsilon_j \sin(\omega_l t - \theta)$ and J_n is the Bessel function of the first kind.

As we pay our attention to the limit-cycle states of the mechanical resonators, we removed all terms in mechanical dynamics except for the constant one and the term oscillating at ω_l . We substitute Eq. (A2) into Eq. (A1) which leads to the following equations of motion for the oscillating part of β_j ($\beta_j \ll B_j$),

$$\begin{aligned} \frac{d\beta_1}{dt} &= -(i\omega_{eff}^1 + \frac{\gamma_{eff}^1}{2} + i\Theta_1)\beta_1 + iJ\beta_2 + i\Theta_1\beta_1^*, \\ \frac{d\beta_2}{dt} &= -(i\omega_{eff}^2 + \frac{\gamma_{eff}^2}{2} + i\Theta_2)\beta_2 + iJ\beta_1 + i\Theta_2\beta_2^*, \end{aligned} \quad (A4)$$

where, $\omega_{eff}^j = \omega_j + \Omega_j$ and $\gamma_{eff}^j = \gamma_m + \Gamma_j$ ($j = 1, 2$) represent the effective frequency and the effective damping of the j th mechanical oscillator ($j = 1, 2$), respectively. The optical spring effect (Ω_j) and optomechanical damping rate (Γ_j) of the mechanical resonator due to the cavity are given by [50]

$$\Omega_j = -\frac{2\kappa(g\alpha^{in})^2}{\omega_l \epsilon_j} Re \left(\sum_n \frac{J_{n+1}(-\epsilon_j) J_n(-\epsilon_j)}{K_{n+1}^{j*} K_n^j} \right), \quad (A5)$$

and

$$\Gamma_j = \frac{2(g\kappa\alpha^{in})^2}{\epsilon_j} \sum_n \frac{J_{n+1}(-\epsilon_j) J_n(-\epsilon_j)}{|K_{n+1}^{j*} K_n^j|^2}. \quad (A6)$$

Here, Ω_j (Γ_j) can be controlled by the external drive signal. If the optomechanical system satisfies the resolved-sideband condition, $\gamma_m, g \ll \kappa \ll \omega_m$ [47, 48], the optical spring effect can be ignored. Further, the effective Hamiltonian of the mechanical modes can be derived as

-
- [1] M. Aspelmeyer, T. J. Kippenberg, and F. Marquardt, Cavity optomechanics, *Rev. Mod. Phys.* **86**, 1391 (2014).
- [2] C. M. Caves, Quantum-Mechanical Radiation-Pressure Fluctuations in an Interferometer, *Phys. Rev. Lett.* **45**, 75 (1980).
- [3] A. Abramovici, W. E. Althouse, R. W. P. Drever, Y. Gürsel, S. Kawamura, F. J. Raab, D. Shoemaker, L. Sievers, R. E. Spero, K. S. Thorne, R. E. Vogt, R. Weiss, S. E. Whitcomb, and M. E. Zucker, LIGO: The laser interferometer gravitational-wave observatory, *Science* **256**, 325 (1992).
- [4] N. Matsumoto, S. B. Cataño-Lopez, M. Sugawara, S. Suzuki, N. Abe, K. Komori, Y. Michimura, Y. Aso, and K. Edamatsu, Demonstration of Displacement Sensing of a mg-Scale Pendulum for mm- and mg-Scale Gravity Measurements, *Phys. Rev. Lett.* **122** 071101 (2019).
- [5] S. Liu, B. Liu, J. Wang, T. Sun, and W. Yang, Realization of a highly sensitive mass sensor in a quadratically coupled optomechanical system, *Phys. Rev. Appl.* **99**, 033822 (2019).
- [6] A. G. Krause, M. Winger, T. D. Blasius, Q. Lin, and O. Painter, A high-resolution microchip optomechanical accelerometer, *Nat. Photonics* **6**, 768 (2012).
- [7] M. Rossi, D. Mason, J. Chen, Y. Tsaturyan, and A. Schliesser, Measurement-based quantum control of mechanical motion, *Nature (London)* **563**, 53 (2018).
- [8] C. M. Caves, K. S. Thorne, R. W. P. Drever, V. D. Sandberg, and M. Zimmermann, On the measurement of a weak classical force coupled to a quantum-mechanical oscillator. I. Issues of principle, *Rev. Mod. Phys.* **52**, 341 (1980).
- [9] S. Schreppler, N. Spethmann, N. Brahms, T. Botter, M. Barrios, and D. M. Stamper-Kurn, Optically measuring force near the standard quantum limit, *Science* **344**, 1486 (2014).
- [10] S. Basiri-Esfahani, A. Armin, S. Forstner, and W. P. Bowen, Precision ultrasound sensing on a chip, *Nat. Commun.* **10**, 132 (2019).
- [11] B. Peng, Ş. K. Özdemir, F. Lei, F. Monifi, M. Gianfreda, G. L. Long, S. Fan, F. Nori, C. M. Bender, and L. Yang, Parity-time-symmetric whispering-gallery microcavities, *Nat. Phys.* **10**, 394 (2014).
- [12] J. Wiersig, Enhancing the Sensitivity of Frequency and Energy Splitting Detection by Using Exceptional Points: Application to Microcavity Sensors for Single-Particle Detection, *Phys. Rev. Lett.* **112** 203901 (2014).
- [13] B. Peng, Ş. K. Özdemir, M. Liertzer, W. Chen, J. Kramer, H. Yılmaz, J. Wiersig, S. Rotter, and L. Yang, Chiral modes and directional lasing at exceptional points, *Proc. Natl. Acad. Sci. USA* **113**, 6845 (2016).
- [14] W. Chen, Ş. K. Özdemir, G. Zhao, J. Wiersig and L. Yang, Exceptional points enhance sensing in an optical microcavity, *Nature (London)* **548**, 192 (2017).
- [15] H. Lü, C. Wang, L. Yang, and H. Jing, Optomechanically Induced Transparency at Exceptional Points, *Phys. Rev. Appl.* **10**, 014006 (2018).
- [16] W. D. Heiss, Exceptional points of non-Hermitian operators, *J. Phys. A-Math. Theor.* **37**, 2455 (2004).
- [17] M. V. Berry, Physics of non-Hermitian degeneracies, *Czech. J. Phys.* **54**, 1039 (2004).
- [18] Z. Lin, H. Ramezani, T. Eichelkraut, T. Kottos, H. Cao, and D. N. Christodoulides, Unidirectional Invisibility Induced by \mathcal{PT} -Symmetric Periodic Structures, *Phys. Rev. Lett.* **106**, 213901 (2011).
- [19] H. Xu, D. Mason, L. Jiang, and J. G. E. Harris, Topological energy transfer in an optomechanical system with exceptional points, *Nature (London)* **537**, 80 (2016).
- [20] H. Jing, S.K. Özdemir, X.-Y. Lü, J. Zhang, L. Yang, and F. Nori, \mathcal{PT} -Symmetric Phonon Laser, *Phys. Rev. Lett.* **113**, 053604 (2014).
- [21] L. Feng, Z. J. Wong, R.-M. Ma, Y. Wang, and X. Zhang, Single-mode laser by parity-time symmetry breaking, *Science* **346**, 972 (2014).
- [22] P. Djourjoe, Y. Pennec, and B. Djafari-Rouhani, Exceptional Point Enhances Sensitivity of Optomechanical Mass Sensors, *Phys. Rev. Appl.* **12**, 024002 (2019).
- [23] J. Ren, H. Hodaei, G. Harari, A. U. Hassan, W. Chow, M. Soltani, D. Christodoulides, and M. Khajavikhan, Ultrasensitive micro-scale parity-time-symmetric ring laser gyroscope, *Opt. Lett.* **42**, 1556 (2017).
- [24] Y.-H. Lai, Y.-K. Lu, M.-G. Suh, Z. Yuan, and K. Vahala, Observation of the exceptional-point-enhanced Sagnac effect, *Nature (London)* **576**, 65 (2019).
- [25] Y.-H. Lai, M.-G. Suh, Y.-K. Lu, B. Shen, Q.-F. Yang, H. Wang, J. Li, S. H. Lee, K. Y. Yang, and K. Vahala, Earth rotation measured by a chip-scale ring laser gyroscope, *Nat. Photonics* **14**, 345 (2020).
- [26] M. P. Hokmabadi, A. Schumer, D. N. Christodoulides, and M. Khajavikhan, Non-Hermitian ring laser gyroscopes with enhanced Sagnac sensitivity, *Nature (London)* **576**, 70 (2019).
- [27] P. P. Khial, A. D. White, and A. Hajimiri, Nanophotonic optical gyroscope with reciprocal sensitivity enhancement, *Nat. Photonics* **12**, 671 (2018).
- [28] W. Heisenberg, Über den anschaulichen Inhalt der quantentheoretischen Kinematik und Mechanik, *Z. Phys.* **43**, 172 (1927).
- [29] L. J. Garay, Quantum gravity and minimum length, *Int. J. Mod. Phys. A* **10**,145 (1995).
- [30] A. Kempf, Information-theoretic natural ultraviolet cut-off for spacetime, *Phys. Rev. Lett.* **103** 231301 (2009).
- [31] M. Bojowald and A. Kempf, Generalized uncertainty principles and localization of a particle in discrete space, *Phys. Rev. D* **86** 085017 (2012).
- [32] G. Veneziano, A stringy nature needs just two constants, *Europhys. Lett.* **2**, 199 (1986).
- [33] D. Amati, M. Ciafaloni, and G. Veneziano, Superstring collisions at planckian energies, *Phys. Lett. B* **197**, 81 (1987).
- [34] D. J. Gross, and P. F. Mende, String theory beyond the Planck scale, *Nucl. Phys. B* **303**, 407 (1988).
- [35] D. Amati, M. Ciafaloni, and G. Veneziano, Can spacetime be probed below the string size? *Phys. Lett. B* **216** 41 (1989).
- [36] K. Konishi, G. Paffuti, and P. Provero, Minimum physical length and the generalized uncertainty principle in string theory, *Phys. Lett. B* **234** 276 (1990).
- [37] G. Amelino-Camelia, Doubly-special relativity: first results and key open problems, *Int. J. Mod. Phys. D* **11** 1643 (2002).
- [38] J. Magueijo and L. Smolin, Generalized Lorentz invari-

- ance with an invariant energy scale, Phys. Rev. D **67**, 044017 (2003).
- [39] G. Amelino-Camelia, L. Freidel, J. Kowalski-Glikman, and L. Smolin, Principle of relative locality, Phys. Rev. D **84**, 084010 (2011).
- [40] F. Scardigli, Generalized uncertainty principle in quantum gravity from micro-black hole Gedanken experiment, Phys. Lett.B **452** 39 (1999).
- [41] S. Das, and E. C. Vagenas, Universality of Quantum Gravity Corrections, Phys. Rev. Lett. **101** 221301 (2008).
- [42] Z.-W. Feng, S.-Z. Yang, H.-L. Li, and X.-T. Zu, Constraining the generalized uncertainty principle with the gravitational wave event GW150914, Phys. Lett. B **768**, 81 (2017).
- [43] U. Jacob, and T. Piran, Neutrinos from gamma-ray bursts as a tool to explore quantum-gravity-induced Lorentz violation, Nat. Phys. **3**, 87 (2007).
- [44] G. Amelino-Camelia, J. Ellis, N. E. Mavromatos, D. V. Nanopoulos, and S. Sarkar, Tests of quantum gravity from observations of γ -ray bursts, Nature **393**, 763 (1998).
- [45] I. Pikovski, M. R. Vanner, M. Aspelmeyer, M. S. Kim, and Č. Brukner, Probing Planck-scale physics with quantum optics. Nat. Phys. **8**, 393 (2012).
- [46] P. Girdhar, A. C. Doherty, Testing generalised uncertainty principles through quantum noise, New J. Phys. **22**, 093073 (2020)
- [47] J. D. Cohen, S. M. Meenehan, G. S. MacCabe, S. Gröblacher, A. H. Safavi-Naeini, F. Marsili, M. D. Shaw, and O. Painter, Phonon counting and intensity interferometry of a nanomechanical resonator, Nature (London) **520**, 522 (2015).
- [48] S. Hong, R. Riedinger, I. Marinkovic, A. Wallucks, S. G. Hofer, R. A. Norte, M. Aspelmeyer, and S. Gröblacher, Hanbury Brown and Twiss interferometry of single phonons from an optomechanical resonator, Science **358**, 203 (2017).
- [49] F. Marquardt, J.G.E. Harris, and S.M. Girvin, Dynamical Multistability Induced by Radiation Pressure in High-Finesse Micromechanical Optical Cavities, Phys. Rev. Lett. **96**, 103901 (2006).
- [50] D.A. Rodrigues, and A.D. Armour, Amplitude Noise Suppression in Cavity-Driven Oscillations of a Mechanical Resonator, Phys. Rev. Lett. **104**, 053601 (2010).
- [51] P . Djorwe, Y . Pennec, and B. Djafari-Rouhani, Frequency locking and controllable chaos through exceptional points in optomechanics, Phys. Rev. E **98**, 032201 (2018).
- [52] M. Li, H. X. Tang, and M. L. Roukes, Ultra-sensitive NEMS-based cantilevers for sensing, scanned probe and very high-frequency applications, Nature Nanotech. **2**, 114 (2007).
- [53] J. D. Thompson, B. M. Zwickl, A. M. Jayich, F. Marquardt, S. M. Girvin and J. G. E. Harris, Strong dispersive coupling of a high-finesse cavity to a micromechanical membrane, Nature **452**, 72 (2008).
- [54] K. L. Ekinci, Y. T. Yang, and M. L. Roukes, Ultimate limits to inertial mass sensing based upon nanoelectromechanical systems, J. Appl. Phys. **95**, 2682 (2004).
- [55] K. Fang, M. H. Matheny, X. Luan, and O. Painter, Optical transduction and routing of microwave phonons in cavity-optomechanical circuits, Nat. Photonics **10**, 489 (2016).